Neutrons from Negative-Muon Capture*

Burns Macdonald, Justo A. Diaz,† Selig N. Kaplan, and Robert V. Pyle

Lawrence Radiation Laboratory, University of California, Berkeley, California

(Received 19 April 1965)

Average neutron-emission and neutron-multiplicity distributions from μ^- capture in Al, Si, Ca, Fe, Ag, I, Au, and Pb were measured. A high-efficiency (54.5% for fission neutrons) cadmium-loaded liquid-scintillator tank was used as the neutron detector. Simple nuclear models with Fermi-gas and Gaussian nucleon-momentum distributions were used to fit the experimental results. A reduced nucleon effective mass was employed to yield the observed average neutron multiplicity, and values were obtained as a function of the width of the assumed nucleon-momentum distributions. Use of the Gaussian momentum distribution obtained in experiments on quasi-elastic scattering gives effective masses ranging from $\approx 0.7\ M_p$ in the lighter nuclei to $\approx 0.45\ M_p$ in the heavier nuclei. An excited-Fermi-gas distribution gives larger effective masses for the lighter nuclei and smaller effective masses for the heavier nuclei than does the Gaussian model. Neither of these models gives good agreement with the neutron-multiplicity distributions, although calculations in which direct neutron emission and nucleon clustering on the nuclear surface are assumed improve the fit. For both the Fermi-gas and Gaussian models, the *average* nuclear excitation energy varies linearly with *average* neutron multiplicity and is relatively insensitive to the model parameters. When the average nuclear excitation is expressed in units of the muon mass reduced by its K-shell binding energy, the result (with the exception of calcium) is constant, 0.18 ± 0.01, over the wide range of atomic numbers covered in the experiment. For Ca⁴⁰ we also made a shell-model calculation using a simple harmonic-oscillator potential. The agreement with the observed average neutron multiplicity is good although perhaps fortuitous.

I. INTRODUCTION

THIS experiment continues an investigation[1] into nuclear-momentum distributions and nucleon effective masses by measurements of the number of neutrons emitted from a nucleus excited by muon capture.

A muon captured into an atomic K shell spends part of its time within the nucleus, and there is a large probability, in not-too-light nuclei, of the muon being captured by a proton according to the weak-interaction process

$$\mu^- + p \rightarrow n + \nu.$$

In competition with this reaction is the muon's decay, $\mu^- \rightarrow e^- + \nu + \bar{\nu}$. (In the elements reported on here, the fractions that decay ran from $\approx 3\%$ in lead to $\approx 40\%$ in aluminum.)

In the capture process the neutrino takes off most of the energy. If the proton is at rest, the neutron recoils with about 5 MeV. Since the proton in the nucleus typically is moving at the time of capture, the recoil energy of the neutron in the rest system of the nucleus is different from 5 MeV. The neutron, and hence the nucleus, will have a distribution of energies $I(Q)$ that depends on the momentum distribution of the capturing proton.

Measurements of the average number of neutrons emitted indicate average nuclear excitations of 10 to 20 MeV. Proton emission is small compared to neutron emission because of the effect of the Coulomb barrier

at these moderate excitations, and photons are given off only when the excitation is below the threshold for particle emission. Thus neutron emission strongly predominates and a knowledge of the numbers of neutrons given out following μ-meson capture yields information about the nuclear-excitation distributions and therefore about the proton-momentum distribution. A more detailed review of the capture process and associated nuclear excitation can be found in Ref. 1.

The earliest effort to describe the nuclear excitation and attendant neutron emission, by Tiomno and Wheeler,[2] has undergone various modifications in order to improve quantitative agreement with experiment.[1,3–6] Most of these modifications find that better agreement is possible if nucleon masses in the nucleus are assumed smaller than unbound nucleon masses. This nucleon characteristic is a consequence of the velocity dependence of nuclear forces that can be approximated by changing the unbound nucleon mass M to a reduced "effective" mass M^*. A number of theoretical approaches to the description of nuclear matter predict effective masses of about one-half the unbound mass.[7–10]

In analyzing an experiment that measures the neutron-multiplicity distribution, we can adjust the effective mass to give agreement between the measured values of average neutron emission and theoretical

---

* Work done under the auspices of the U. S. Atomic Energy Commission.

† Present address: Physics Department, Ottawa University, Ottawa, Kansas.

[1] S. N. Kaplan, B. J. Moyer, and R. V. Pyle, Phys. Rev. 112, 968 (1958).

[2] J. Tiomno and J. A. Wheeler, Rev. Mod. Phys. 21, 153 (1949).
[3] J. M. B. Lang, Proc. Phys. Soc. (London) A65, 995 (1952).
[4] Francis T. Cole, Ph.D. thesis, Cornell University, 1953 (unpublished).
[5] Paul Singer, Nuovo Cimento, 23, 669 (1962).
[6] Paul Singer, Phys. Rev. 124, 1602 (1961).
[7] M. H. Johnson and E. Teller, Phys. Rev. 98, 783 (1955).
[8] K. A. Brueckner and J. L. Gammell, Phys. Rev. 109, 1023 (1958).
[9] V. Weisskopf, Nucl. Phys. 3, 423 (1957).
[10] H. A. Bethe, Phys. Rev. 103, 1353 (1956).

predictions for various choices of the nucleon-momentum distributions. However, it was hoped that the resulting distribution of neutron multiplicities, being generally different for these various models, would allow a more definitive picture of the capture process.

Some details of the nuclear excitations that can be inferred from neutron-multiplicity measurements are also of interest in muon-capture-rate calculations, the capture rate being a sensitive function of the excitation. A reduced mass $M^* = M/2$ has been used to improve agreement between experimental capture rates in medium and heavy nuclei and calculations involving universal-Fermi-interaction coupling constants.[11,12]

The first high-efficiency measurement of the distribution of multiplicities was made for silver and lead,[1] in which cosmic-ray muons were used and a large cadmium-loaded liquid-scintillator tank served as a high-efficiency neutron detector. There was considerable advantage to be gained, in terms of counting rate and purity of beam, by using muons from the 184-in. cyclotron; this experiment was carried out with the same neutron detector for eight targets ranging from aluminum to lead.

II. THEORY

A. Nuclear Excitation

In calculating the nuclear-excitation distribution we assume the same form for the capture probability used in Ref. 1,

$$\omega = K' \int d^3\mathbf{p}\, d^3\mathbf{p}\, d^3\mathbf{q}\ f(\mathbf{p})[1 - g(\mathbf{q})]\delta(\mathbf{p}_\nu + \mathbf{q} - \mathbf{p})$$
$$\times \delta(E_0 - p_\nu c - Q), \quad (1)$$

in which K' is a constant; $f(\mathbf{p})$ and $g(\mathbf{q})$, obtained from the ground-state nuclear wave function, are the probabilities per unit volume of momentum space of finding a proton of momentum $\mathbf{p}$ and a neutron of momentum $\mathbf{q}$; the factor $[1 - g(\mathbf{q})]$ is contributed by the Pauli exclusion principle; p_ν is the neutrino momentum; Q is the excitation of the product nucleus $(Z-1, A)$; and E_0 is the total energy available for excitation: the rest energy of the muon reduced by both its K-shell binding energy, and the $(Z-1, A)$, (Z,A) mass difference. The transition probability can be expressed in terms of the nuclear-excitation distribution $I(Q)$ as

$$\omega \propto \int I(Q) dQ.$$

We can therefore derive $I(Q)$ [except for a normalization constant given by $\int I(Q)dQ = 1$] by partial integration of (1) to obtain an expression involving only the variable Q.

1. Fermi-Gas Model

The momentum-distribution functions for a degenerate Fermi gas are taken to be

$$f(\mathbf{p}) = 1/\{1 + \exp[(p^2 - p_0^2)/2M\theta_f]\},$$
$$g(\mathbf{q}) = 1/\{1 + \exp[(q^2 - q_0^2)/2M\theta_f]\}, \quad (2)$$

where θ_f is the Fermi temperature in energy units (MeV), and p_0 and q_0 are the proton and neutron Fermi momenta for the target and product nuclei, respectively.

Following Ref. 1 we obtain for $I(Q)$

$$I(Q) = \frac{2\theta_f K(E_0 - Q)}{1 - \exp(-Q/\theta_f)} \ln\left[\frac{1 + \exp[(a+Q)/2\theta_f]}{1 + \exp[(a-Q)/2\theta_f]}\right], \quad (3)$$

where

$$a = \frac{(q_0^2 + p_0^2)}{2M^*} - \frac{p_\nu^2}{4M^*} - \frac{M^*[E_0 - p_\nu c - (q_0^2 - p_0^2)/2M^*]^2}{p_\nu^2},$$

and the normalization constant K is determined by $\int I(Q)dQ = 1$. The effective nucleon mass is M^*, whose value will be derived by optimizing the agreement between this model and the observed average neutron emission.

2. Gaussian Model

If a Gaussian momentum distribution of the nucleons is assumed, then

$$f(\mathbf{p}) = \exp(-p^2/\alpha^2),$$
$$g(\mathbf{q}) = \exp(-q^2/\alpha^2), \quad (4)$$

where α gives the width of the momentum distribution and is determined experimentally from quasi-elastic scattering. The nuclear-excitation distribution derived from Eq. (1) then becomes[5]

$$I(Q) = K'(E_0 - Q)$$
$$\times \{\exp[-f_1(Q)] - \tfrac{1}{2}\exp[-2f_2(Q)]\}, \quad (5)$$

where

$$f_1(Q) = \alpha^{-2}\{\tfrac{1}{4}(E_0 - Q)^2 - M^*Q + M^{*2}Q^2/(E_0 - Q)^2\}$$
$$f_2(Q) = \alpha^{-2}\{\tfrac{1}{4}(E_0 - Q)^2 + M^{*2}Q^2/(E_0 - Q)^2\},$$

and K' is a normalization constant.

3. Shell Model

Nuclear-excitation distributions can also be calculated from a shell model and $I(Q)$ then becomes a discrete spectrum of energies. Luyten, Rood, and Tolhoek[13] have calculated $I(Q)$ for Ca^{40} for a simple harmonic-oscillator shell model. This simple model is, however, not suitable for evaluating neutron emission since it

[11] Richard R. Silbar, Phys. Rev. 134, B542 (1964).
[12] J. S. Bell and J. Løvseth, Nuovo Cimento 32, 433 (1964).

[13] J. R. Luyten, H. P. C. Rood, and H. A. Tolhoek, Nucl. Phys. 41, 236 (1963).

TABLE I. Isotopic abundances, nuclear mass differences, muon binding energies, total muon-disappearance rates, and decay rates.

Target	Atomic mass number	Abundance[a]	Product nucleus	$M(Z-1,A)-M(Z,A)$[b] (MeV)	B_μ°[c] (MeV)	$\lambda \times 10^{-5d}$ (sec^{-1})	$\lambda_d \times 10^{-5e}$ (sec^{-1})	λ_d/λ
$_{13}$Al	27	1.000	$_{12}$Mg	3.129	0.463	11.32	4.54	0.401
$_{14}$Si	28	0.922	$_{13}$Al	5.151	0.535	12.06	4.54	0.376
$_{20}$Ca	40	0.970	$_{19}$K	1.833	1.054	29.6	4.54	0.153
$_{26}$Fe	56	0.917	$_{25}$Mn	4.220	1.72	51.0	4.45	0.087
$_{47}$Ag	107	0.514	$_{46}$Pd	0.546 ⎫	4.76	118.5	4.16	0.0351
$_{47}$Ag	109	0.486	$_{46}$Pd	1.624 ⎭				
$_{53}$I	127	1.000	$_{52}$Te	1.200	5.80	116.1	4.13	0.0356
$_{79}$Au	197	1.000	$_{78}$Pt	1.26	10.10	145.8	3.8	0.0261
$_{82}$Pb	206	0.236	$_{81}$Tl	2.02 ⎫	10.66	134.9	3.8	0.0282
$_{82}$Pb	207	0.226	$_{81}$Tl	1.953 ⎬				
$_{82}$Pb	208	0.523	$_{81}$Tl	5.506 ⎭				

[a] Gladys H. Fuller, in *Nuclear Data Tables*, edited by K. Way (U. S. Government Printing Office, Washington 25, D. C., 1959) p. 66. Abundances not quoted in our table were neglected. The sum of those quoted for an element were normalized to unity in our calculations.
[b] L. A. König, J. H. E. Mattauch, and A. H. Wapstra, Nucl. Phys. 31, 18 (1962).
[c] Kenneth W. Ford and John G. Wills, Calculated Properties of Mu-Mesonic Atoms, Los Alamos Scientific Laboratory Report LAMS-2387, 1959 (unpublished).
[d] Al, Si, Ca: J. C. Sens, Phys. Rev. 113, 679 (1959); Fe, Ag, Au, Pb: S. N. Kaplan, J. S. Baijal, J. A. Diaz, G. Kojoian, and R. V. Pyle, Bull. Am. Phys. Soc. 7, 489 (1962); Iodine: T. A. Filipas, R. Palit, R. T. Siegel, and R. E. Welsh, Phys. Letters 6, 118 (1963).
[e] R. W. Huff, Ann. Phys. (N.Y.) 16, 288 (1961).

predicts nuclear excitations in multiples of $\hbar\omega_0$ (≈ 10 MeV) only. We have extended this calculation using their transition probability and employing Nilsson's Hamiltonian,[14] which splits the simple harmonic-oscillator energy levels with terms proportional to $\mathbf{l}\cdot\mathbf{s}$ and to l^2.

$$\mathcal{3C} = \hbar\omega_0 - 2\hbar\omega_0\chi\mathbf{l}\cdot\mathbf{s} - \hbar\omega_0\chi\mu l^2$$

B. Neutron Emission

Nuclear de-excitation is assumed to occur by neutron boil-off and is treated exactly as in Ref. 1, which gives the probability of emission of at least ν neutrons N_ν as

$$N_\nu = 1 - \exp[-(Q-B_\nu)/\theta_n]$$
$$\times \sum_{n=0}^{2\nu-3} [(Q-B_\nu)/\theta_n]^n (n!)^{-1}, \quad (6)$$

where B_ν is the binding energy of the first ν neutrons to be emitted, and θ_n is the temperature of the compound nucleus and is assumed to be a constant in the derivation of N_ν. Variation of θ_n over a reasonable range of values has only a small effect on the neutron multiplicities.

The probability for emission of just ν neutrons by a nucleus with a distribution of excitations, $I(Q)$, is, therefore,

$$P_\nu = \int_{B_\nu}^{E_0} N_\nu I(Q)dQ - \int_{B_{\nu+1}}^{E_0} N_{\nu+1} I(Q)dQ. \quad (7)$$

The integrals were evaluated numerically for the various excitation distributions. The constants used are given in Tables I and II. The values of P_ν were then averaged over the natural isotopic abundances of the targets (Table I). The values obtained are those ex-

pected with a 100%-efficiency detector. To compare with experimental values of the neutron multiplicities, we converted the P_ν's to the distribution (F_n) expected with a detector of efficiency e ($e = 0.545$).

$$F_n = e^n \sum_{\nu=n}^{\infty} P_\nu(1-e)^{\nu-n}(\nu!/n!(\nu-n)!). \quad (8)$$

Direct neutron emission has been considered by several authors and will be discussed later.

III. EXPERIMENTAL PROCEDURE

A. Detection System

A negative beam of particles was produced within the Berkeley 184-in. cyclotron. Particles of 200-MeV/c momentum were selected by a magnet system and detected by a scintillation-counter telescope. The counter
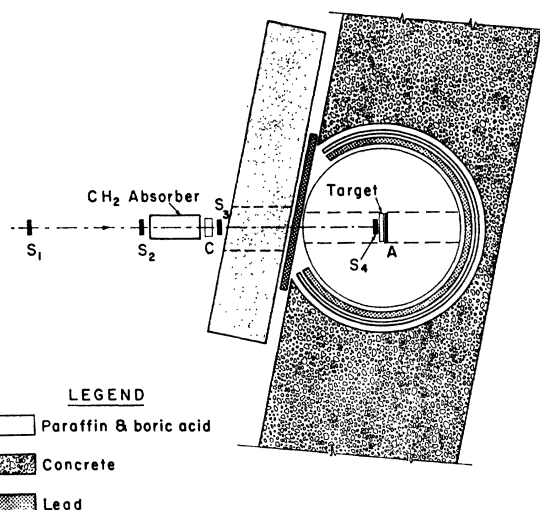

LEGEND
☐ Paraffin & boric acid
▨ Concrete
▨ Lead

FIG. 1. Experimental arrangement of the counter telescope and cadmium-loaded liquid-scintillator tank.

[14] Sven Gösta Nilsson, Kgl. Danske Videnskab. Selskab, Mat. Fys. Medd. 29, No. 16 (1955).

TABLE II. Neutron separation energies.

Target nucleus	→	Product nucleus		Atomic-mass number and neutron separation energies (MeV)[a]								
$_{13}$Al	→	$_{12}$Mg	A	27	26	25	24	23				
				6.437	11.097	7.331	16.535	13.442				
$_{14}$Si	→	$_{13}$Al	A	28	27	26	25	24				
				7.723	13.069	11.344	17.090	12.9[b]				
$_{20}$Ca	→	$_{19}$K	A	40	39	38	37	36	35	34	33	
				7.798	13.079	12.030	15.154[b]	12.835	17.6[b]	15.8[b]	22.0[b]	
$_{26}$Fe	→	$_{25}$Mn	A	56	55	54	53	52	51	50		
				7.270	10.220	8.940	12.049	10.529	13.47	12.3[b]		
$_{47}$Ag	→	$_{46}$Pd	A	109	108	107	106	105	104	103	102	101
				6.24[c]	9.08[c]	6.39[c]	9.41[c]	7.409[c]	9.80[c]	7.62[c]	10.26[c]	9.01[c]
$_{53}$I	→	$_{52}$Te	A	127	126	125	124	123	122	121	120	
				6.353[c]	9.099[c]	6.577[c]	9.417[c]	6.789[c]	9.9[b]	7.6[b]	10.2[b]	
$_{79}$Au	→	$_{78}$Pt	A	197	196	195	194	193	192	191	190	
				5.86	7.92	6.21	8.55	6.3	7.8[b]	6.4[b]	8.3[b]	
$_{82}$Pb	→	$_{81}$Tl	A	208	207	206	205	204	203	202	201	200
				3.83	6.80	6.56	7.54	6.62	7.88	6.79	8.2[b]	6.5[b]

[a] From L. A. König, J. H. E. Mattauch, and A. H. Wapstra, Nucl. Phys. 31, 18 (1962), except as noted.
[b] A. G. W. Cameron, Chalk River Report CRP-690, 1957 (unpublished).
[c] V. A. Kravtsov, Nucl. Phys. 41, 330 (1963).

telescope (Fig. 1) was made of $\frac{1}{4}$-in.-thick plastic scintillators except for the 2-in.-thick water Čerenkov counter C and the $\frac{1}{2}$-in.-thick plastic anticounter A. Because of their smaller velocity, negative muons were stopped by an amount of CH_2 absorber that allowed the muons to pass through and stop in the targets. The effect of a small number of electrons in the beam was eliminated by a water Čerenkov counter in anticoincidence with the telescope.

The number distribution of neutrons emitted after μ^- capture was measured in a large (30 in. high, 30 in. diam.) cadmium-loaded liquid scintillator tank.[15] The neutrons were thermalized and captured in the cadmium with a capture lifetime of 7.8 μsec, and the resulting gamma-ray-scintillation pulses were detected by an array of photomultipliers viewing the scintillation tank. The detection efficiency for a single neutron was about 55%.
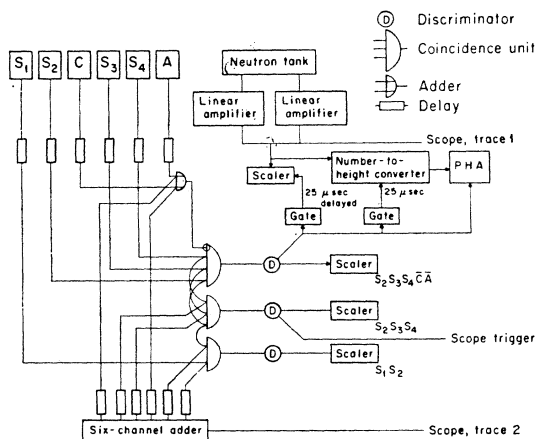
A block diagram of the electronics is given in Fig. 2. The resolution times of the coincidence circuits were about 10 nsec. The beam was monitored with S_1 and S_2 in coincidence. A stopping particle (S_2, S_3, and S_4 in coincidence and the sum of C and A in anticoincidence) triggered a 30-μsec gate which was delayed by 2 μsec to eliminate prompt pulses associated with muon decay or capture in the target.

Neutron pulses occurring during the gate times were fed into a number-to-height converter and stored in a 10-channel pulse-height analyzer. This method gave immediate multiplicity information during the run, but more detailed information was obtained from the photographs of oscilloscope traces. The neutron-detector pulses were displayed on a 35-μsec exponential sweep $x = x_0[1 - \exp(-t/7.8)]$ to give an equal density of pulses along the trace. Another (linear) trace contained the delayed and added outputs from the six telescope counters displayed in sequence (Fig. 3).

The tank background was continuously sampled by a scaler that was gated on for 25 μsec after a suitable delay following each telescope pulse. This sampling tech-

FIG. 2. Block diagram of electronics.

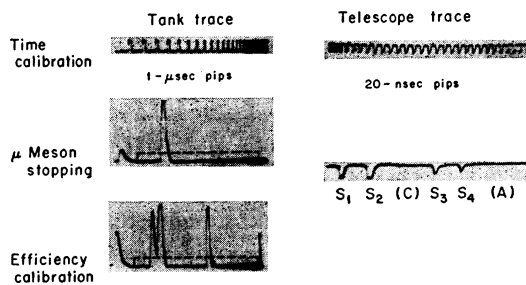[15] Donald A. Hicks, John Ise, Jr., and Robert V. Pyle, Phys. Rev. 101, 1016 (1956).

FIG. 3. Typical oscilloscope traces. For the tank trace, the dotted line represents the minimum height accepted and the time during which the neutron pulses were counted. On the telescope trace a muon stopping is signaled by the presence of pulses from counters S_2, S_3, and S_4, and the absence of Čerenkov and anticounter pulses (C and A).

nique was periodically compared with and calibrated against background obtained on film.

B. Beam Quality

Since the higher neutron multiplicities can be strongly affected by pions, considerable attention was directed to reducing to a minimum and measuring the pion contamination in the muon beam stopping in the targets.

In order to estimate an upper limit to the pion contamination, a positive beam was stopped in a scintillator target and the π^+-μ^+ decays were counted as a function of CH_2 absorber thickness (Fig. 4.). The addition of 2.5 in. of CH_2 reduced the π-decay rate to less than 10^{-3} of its peak value. For greater thicknesses, statistically significant π decays were undetectable with our apparatus, but the number of π's is presumed to continue decreasing with the further addition of absorber. (The μ peak is 5 in. of CH_2 beyond the π peak.)

The reversal of the field directions of all magnets, including that of the cyclotron, produced a negative beam with the same geometrical properties. A negative beam of maximum intensity had a μ/π ratio of about $\frac{1}{7}$. Changes in the position of the cyclotron's internal target, however, strongly influence the beam composition as well as the intensity; this is because pions are produced in the target, whereas the muons originate from π decay and have a much more diffuse source. With some sacrifice in beam intensity it was possible to improve greatly the μ/π ratio.

Figure 5, a differential range curve of the final meson beam, shows the stoppings in a 1-in. thick carbon target inside the neutron detector. A comparison of this
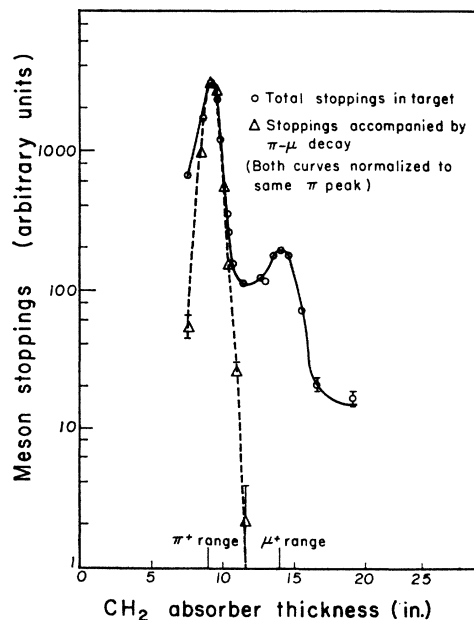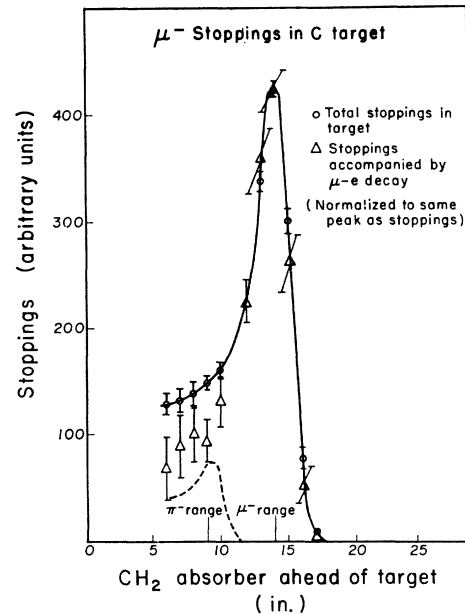

FIG. 5. Negative-muon stoppings in a carbon target.

curve with the one of μ^--e^- decay as a function of absorber thickness (normalized to the same number of stoppings at the μ^- peak) shows that π's comprise less than 20% of the total beam. (The μ^- intensity was reduced to one-seventh.) Combining this information with the π^+ result, we estimate that the fraction of π's stopping in the target is less than 0.0001 with 13 in. of CH_2 absorber. This fraction is small enough to preclude any significant contribution to either the average neutron production or the neutron-multiplicity distributions.

C. Data-Collection Procedure

Eight targets were chosen so as to span a wide range of atomic weights, be monoisotopic where possible, and permit comparison with the results of the previous cosmic-ray experiment. All targets were 7 in. in diameter (the size of the beam tube) and of thicknesses sufficient to stop all of the muons (about 10 g/cm² CH_2 equivalent).

The beam level was reduced to give an average of not more than 0.1 background "neutron" pulse per stopping muon. This background rate corresponded to a muon stopping rate of about 2/min.

For each element, six to twenty 1-h target runs, alternated with background runs, were made. In addition, several runs were made with no target in place to correct for muons stopping in the last counter (S_4).

D. Calibrations

The neutron-detection efficiency was calibrated at frequent intervals by replacing the target assembly

FIG. 4. Positive-meson stoppings in the scintillator target.

TABLE III. Experimentally observed neutron multiplicities (uncorrected data).

Target	Neutron gate times (μsec)	Efficiency	Average background (pulses per 30-μsec sweep)	Total events	Multiplicity distribution						
					f_0	f_1	f_2	f_3	f_4	f_5	f_6
Al	2.5 to 31.0	0.495±0.014	0.102	1492	912	471	81	26	1	0	1
Si[a]	2.5 to 29.5	0.553±0.015	0.082	657	439	186	28	1	1	1	1
Ca[a]	2.5 to 29.5	0.553±0.015	0.078	1846	1154	605	73	10	4	0	0
Fe	1.5 to 31.0	0.545±0.015	0.105	1426	705	559	132	26	2	2	0
Ag	1.5 to 31.0	0.545±0.015	0.129	897	317	384	146	38	9	2	1
I	1.5 to 31.0	0.545±0.015	0.122	909	351	405	108	35	9	1	0
Au	1.5 to 31.0	0.545±0.015	0.114	1192	408	510	198	52	19	4	1
Au[a]	1.5 to 29.5	0.608±0.017	0.097	535	201	199	101	22	9	3	0
Pb	1.5 to 31.0	0.545±0.015	0.117	720	235	325	113	37	10	0	0
Target out	1.5 to 31.0	0.545±0.015	0.093	30	18	12					
Target out[a]	1.5 to 29.5	0.599±0.017	0.089	25	12	13					

[a] Data taken during a later cyclotron run.

with a fission chamber containing Cf^{252}. This isotope yields an average of 3.87±0.08 neutrons per spontaneous fission.[16] We assume that boil-off neutrons from μ^- capture have roughly the same energy spectrum as the fission neutrons. For a somewhat different geometry, Monte Carlo calculations gave the following energy dependence for neutron thermalization and capture efficiency of the tank: 99%, 95%, 89%, and 84% for 1-, 3-, 5-, and 7-MeV neutrons, respectively.[15]

The oscilloscope-sweep speeds were calibrated periodically with a crystal-controlled oscillator.

IV. DATA ANALYSIS

The data on film were transferred to punched cards by means of a digitized scanning projector. With the data in this form it was a simple matter with a computer for us to vary pulse height and timing criteria in order to normalize and optimize data relative to background.

Tank-trace pulses were accepted for 30 μsec beginning either 1.5 or 2.5 μsec after the prompt-pulse time. The longer delays were used for the three lightest elements (Table III) in order to reduce the fraction of μ-decay electrons occurring within the neutron gate. The choice of the minimum acceptable pulse height was determined by the sharp rise in background for lower values and the gradual lessening of neutron-detection efficiency for higher values.

The time distribution of neutrons from the Cf^{252} fission-chamber-calibration runs is given in Fig. 6. (The fall-off at the earliest time is due to the time taken for the neutrons to thermalize.) Comparison of the fission-chamber data with the time distribution of tank pulses from μ capture verifies that these pulses are due to neutrons.

A background correction to the measured multiplicity distribution was made for every target run and used the counter background data taken on each of the runs.

These counter data were calibrated against frequent background measurements recorded on film, which showed that these background pulses were randomly (Poisson) distributed in time. From the target-out measurements we determined that the fraction of muons not stopping in the target was 0.07±0.01. A further correction was made for muon decay. The fraction that decays is λ_d/λ (Table I), where λ_d is the decay rate, and the total disappearance rate λ is the sum of λ_d and the capture rate λ_c. In aluminum and silicon it was also necessary to correct for decay electrons detected during the neutron gate time. This correction reduced the number of single-neutron observations in Al and Si by $\approx 7\%$.
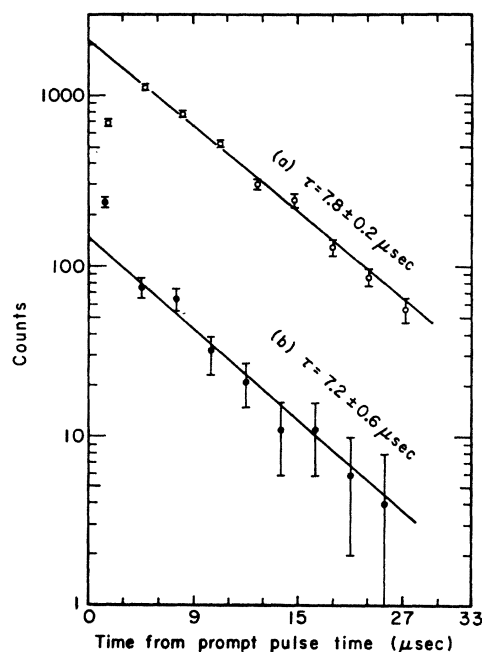

FIG. 6. Time distribution of delayed pulses from (a) Cf^{252} fission-chamber-calibration runs, and (b) μ^- stoppings in silicon. Background has been subtracted.

[16] B. C. Diven, H. C. Martin, R. F. Taschek, and J. Terrell, Phys. Rev. 101, 1012 (1956).

TABLE IV. Corrected experimental results.

Target	Average multiplicity, (n)	F_0	F_1	Multiplicity distribution (adjusted to 0.545 efficiency)					
				F_2	F_3	F_4	F_5	F_6	F_7
Al	1.262±0.059	0.449±0.027	0.464±0.028	0.052±0.013	0.036±0.007	−0.0023±0.004	−0.001±0.004	0.003±0.004	
Si	0.864±0.072	0.611±0.042	0.338±0.042	0.045±0.018	−0.002±0.008	0.003±0.005	0.002±0.005	0.003±0.006	
Ca	0.746±0.032	0.633±0.021	0.335±0.022	0.025±0.009	0.004±0.006	0.003±0.003			
Fe	1.125±0.041	0.495±0.018	0.416±0.019	0.074±0.011	0.014±0.005	−0.0001±0.003	0.002±0.003		
Ag	1.615±0.060	0.360±0.021	0.456±0.023	0.144±0.017	0.031±0.009	0.007±0.005	0.002±0.004	0.001±0.003	
I	1.436±0.056	0.396±0.021	0.474±0.023	0.087±0.015	0.035±0.009	0.007±0.005	0.0002±0.004		
Au	1.662±0.044	0.370±0.015	0.425±0.016	0.156±0.012	0.032±0.006	0.014±0.004	0.003±0.003	0.0003±0.003	
Pb	1.709±0.066	0.324±0.022	0.483±0.025	0.137±0.018	0.045±0.010	0.011±0.006			
Ag[a]	1.60±0.18	0.389±0.100	0.455±0.075	0.120±0.035	0.030±0.015	0.001±0.003	0.009±0.006	0.000±0.007	0.010±0.00
Pb[a]	1.64±0.16	0.348±0.100	0.479±0.057	0.137±0.027	0.018±0.012	0.010±0.005	0.005±0.004	0.003±0.002	0.002±0.002

[a] Results of Kaplan, Moyer, and Pyle (Ref. 1).

V. RESULTS AND DISCUSSION

A. Experimental Results

Uncorrected values of the experimentally observed neutron multiplicities are given in Table III. Values corrected for background, target-out, and decay and reduced to a common detection efficiency (0.545) are given in Table IV. The neutron-multiplicity results of Ref. 1, which reported the same neutron detector and fission-chamber-calibration method as used in the present experiment, are given at the bottom of this table. The agreement with this experiment is good, both for average neutron emission and for multiplicity distributions. A summary of previous experimental results for average multiplicities for our targets is given in Table V.

TABLE V. Average neutron multiplicities from previous experimental results.

Element	Average multiplicity	Source
Al	0.95±0.17[a]	Widgoff (1953)[b]
Ca	0.40±0.4	Conforto and Sard (1952)[c,d]
Ag	1.60±0.18	Kaplan, Moyer, and Pyle (1958)[e]
I	1.7 ±0.4	Winsberg (1954)[f]
Pb	1.96±0.72	Groetzinger, Berger, and McClure (1951)[g]
Pb	2.1 ±0.5	Crouch and Sard (1952)[h,d]
Pb	1.5 ±0.4	Conforto and Sard (1952)[c,d]
Pb	2.14±0.13[a]	Widgoff (1953)[b]
Pb	1.5 ±0.4	Jones (1957)[i]
Pb	1.64±0.16	Kaplan, Moyer, and Pyle (1958)[e]

[a] Statistical errors only.
[b] See M. Widgoff, Phys. Rev. 90, 891 (1953).
[c] See A. M. Conforto and R. D. Sard, Phys. Rev. 86, 465 (1952).
[d] These values and errors are as quoted by R. D. Sard and M. F. Crouch, Progress in Cosmic Ray Physics (North-Holland Publishing Company, Amsterdam, 1954), Vol. II, 3.
[e] See Ref. 1.
[f] See L. Winsberg, Phys. Rev. 95, 205 (1954).
[g] See G. Groetzinger, M. J. Berger, and G. W. McClure, Phys. Rev. 81, 969 (1951).
[h] See M. F. Crouch and R. D. Sard, Phys. Rev. 85, 120 (1952).
[i] See D. R. Jones, Phys. Rev. 105, 1591 (1957).

17 Burns Macdonald, Ph.D. thesis, Lawrence Radiation Laboratory Report UCRL-11243, 1964 (unpublished).

A detailed description of the error analysis can be found in Ref. 17.

B. Comparison of Experiment with Theory

The following calculations of neutron emission are given without including effects of direct emission since it is not clear what these corrections should be. (Calculations of direct emission for calcium range from 25%, by Dolinsky and Blokhintsev,[18] to ≈2%, inferred from Lubkin.[19]) Results that include Singer's direct-emission corrections for the heavy elements are given at the end of Sec. V.

We have investigated two forms of the nucleon-momentum distribution, a Gaussian and a Fermi gas, in our calculation of neutron emission from μ^- catpure. Values of average neutron emission and multiplicity distributions from these models are functions of: (a) the momentum-distribution width ($\alpha^2/2M$ for the Gaussian, or θ_f for the Fermi gas), and (b) the nucleon effective mass M^*. As a first step we made a wide range of choices for the distribution width, and for each choice calculated the M^* that gave the measured average neutron multiplicity. For this M^* a comparison was then made of the predicted multiplicity distribution (P_0, P_1, $\cdots$), with the measured values ($F_0 \pm \delta F_0$, $F_1 \pm \delta F_1$, $\cdots$); and the standard goodness-of-fit parameter $\chi^2 = \sum_n [(P_n - F_n)/\delta F_n]^2$ was determined. (The χ^2 was generally associated with three to four degrees of freedom. For example, a value of $\chi^2 \approx 3.4$ for four degrees of freedom corresponds to a probability of 50% that chance gives no better fit.)

Figure 7 shows typical profiles of M^* and χ^2 plotted against the momentum-width parameter. Because χ^2 is not a sensitive function of the width parameter, the model cannot determine both the effective mass and the width of the momentum distribution. Therefore, in ascertaining an effective nucleon mass we must rely on other sources for nucleon-momentum-distribution data. Such data come from a variety of measurements on interactions of high-energy radiation with light nuclei, and for a simple Gaussian distribution yield a width parameter $\alpha^2/2M$ that ranges from about 14 to 20 MeV,

18 E. I. Dolinsky and L. D. Blokhintsev, Nucl. Phys. 10, 527 (1959).
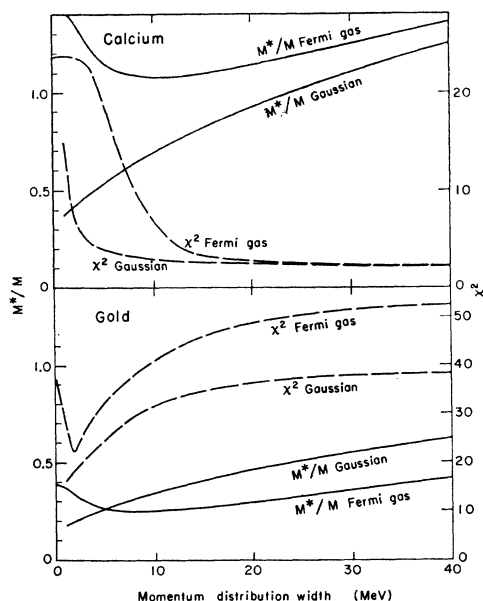19 Elihu Lubkin, Ann. Phys. (N. Y.) 11, 44 (1960).

FIG. 7. The effective mass M^* required to give the experimental $\langle n \rangle$, and the corresponding fit $\langle \chi^2 \rangle$ with the experimental multiplicity distribution, as functions of the momentum-width parameter (θ_f for Fermi gas, or $\alpha^2/2M$ for the Gaussian). For calcium and gold.

the preponderance of data being closer to the larger value.[20] For all of our elements χ^2 is essentially constant in this range whereas M^* generally increases by $\approx 15\%$ (Fig. 7).

The momentum-distribution function for a 20-MeV Gaussian is shown in Fig. 8. Also plotted is a Fermi-gas distribution ($\theta_f = 12$ MeV) having the same mean-square momentum as the 20-MeV Gaussian, and a completely degenerate Fermi-gas distribution.

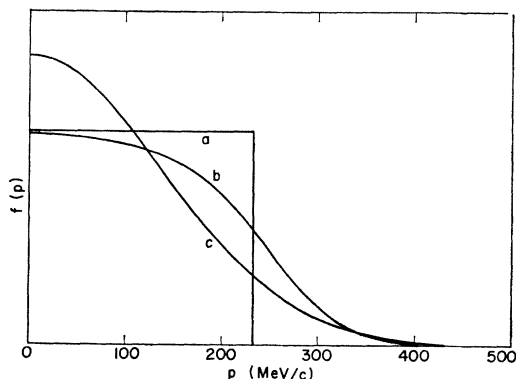Figure 9 gives the nuclear-excitation distributions

FIG. 8. Nucleon-momentum distributions. (a) Fermi gas (gold), $\theta_f = 0$ MeV; (b) Fermi gas (gold), $\theta_f = 12$ MeV; (c) Gaussian, $\alpha^2/2M = 20$ MeV.

[20] L. S. Azhgirey, I. K. Vzorov, V. P. Zrelov, M. G. Mescheryakov, B. S. Neganov, R. M. Ryndin, and A. F. Shabudin, Nucl. Phys. 13, 258 (1959). Reference to earlier work is given in this paper.

TABLE VI. Fermi-gas distribution, $\theta_f = 0$ MeV. The effective mass that gives the experimental average multiplicity χ^2 and the predicted multiplicity distribution.

Target	Effective mass M^*/M	χ^2	Multiplicity distribution			
			P_0	P_1	P_2	P_3
Al	0.74	41.9	0.415	0.483	0.102	
Si	0.95	17.6	0.534	0.461	0.005	
Ca	1.39	23.5	0.593	0.407		
Fe	0.76	18.9	0.460	0.467	0.073	
Ag	0.49	9.9	0.337	0.464	0.180	0.019
I	0.50	29.5	0.375	0.473	0.146	0.005
Au	0.38	36.8	0.329	0.459	0.190	0.023
Pb	0.36	22.9	0.315	0.461	0.203	0.022

$I(Q)$ for the above momentum distributions. (Because M^* in each case was chosen to give the experimental $\langle n \rangle$ all the average nuclear excitations for these curves have substantially the same value.)
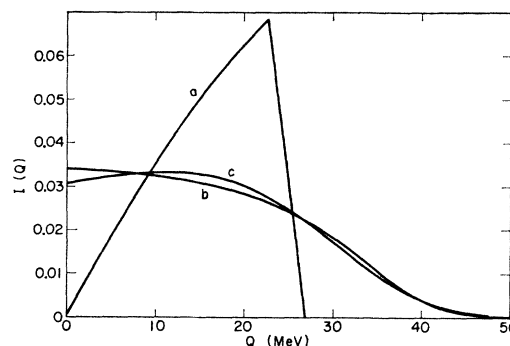

FIG. 9. Nuclear excitation distribution from μ^- capture in gold. The effective mass in each case has been chosen so as to give the experimental average multiplicity. (a) Fermi gas (gold), $\theta_f = 0$ MeV; (b) Fermi gas (gold), $\theta_f = 12$ MeV; (c) Gaussian $\alpha^2/2M = 20$ MeV.

Values of M^*/M, χ^2, and the predicted multiplicity distributions for Fermi-gas-momentum distributions with $\theta_f = 0$ and 12 MeV are given in Tables VI and VII. Gaussian-momentum-distribution results with $\alpha^2/2M = 20$ MeV are given in Table VIII. The fits with the observed multiplicity distributions are not good, except for silicon and calcium, which give good agreement for

TABLE VII. Fermi-gas distribution, $\theta_f = 12$ MeV. The effective mass that gives the experimental average multiplicity χ^2 and the predicted multiplicity distribution.

Target	Effective mass M^*/M	χ^2	Multiplicity distribution				
			P_0	P_1	P_2	P_3	P_4
Al	0.60	40.0	0.465	0.399	0.119	0.017	
Si	0.81	2.6	0.573	0.383	0.043		
Ca	1.03	5.0	0.613	0.367	0.020		
Fe	0.60	10.9	0.505	0.385	0.102	0.008	
Ag	0.35	25.3	0.404	0.370	0.172	0.049	0.005
I	0.37	42.0	0.441	0.373	0.149	0.035	0.002
Au	0.25	43.8	0.403	0.359	0.175	0.055	0.007
Pb	0.24	39.4	0.389	0.364	0.182	0.056	0.008

TABLE VIII. Gaussian distribution, $\alpha^2/2M = 20$ MeV. The effective mass that gives the experimental average multiplicity χ^2 and the predicted multiplicity distribution.

Target	Effective mass M^*/M	χ^2	P_0	Multiplicity distribution P_1	P_2	P_3	P_4	P_5
Al	0.59	38.0	0.469	0.393	0.118	0.020		
Si	0.73	1.9	0.579	0.372	0.048	0.001		
Ca	0.92	2.5	0.621	0.352	0.027			
Fe	0.63	10.6	0.510	0.379	0.100	0.011		
Ag	0.45	23.6	0.404	0.373	0.169	0.048		
I	0.54	38.3	0.440	0.377	0.146	0.034	0.003	
Au	0.46	36.4	0.399	0.366	0.175	0.053	0.007	0.001
Pb	0.48	34.5	0.383	0.372	0.183	0.053	0.008	

all $\theta_f > 7$ to 10 MeV. (Examples are shown in Fig. 7). This better agreement for silicon and calcium is probably due to their lower neutron yields which are attended by less stringent parameter-fitting requirements.

The harmonic-oscillator shell-model calculation of the excitation of Ca^{40} (Fig. 10) gives a value for the average multiplicity, $\langle n \rangle = 0.744$, which is in good agreement with the experimental results, $\langle n \rangle = 0.746 \pm 0.032$. The calculated average excitation, $\langle Q \rangle = 11.15$ MeV, is close to $Q = 11.7$ MeV, derived from the Fermi gas and Gaussian models and the measured $\langle n \rangle$. The agreement of this shell-model calculation is interesting but is probably accidental, since the threshold for emission of the first neutron, $Q + M(Z-1, A)c^2 - M(Z,A)c^2 = 9.63$ MeV, happens to fall in the narrow range defined by the two most frequent transitions.

Effective masses of 0.540 and 0.389 for I and Au, respectively, have been calculated by Clementel and Villi from experimental values of nuclear-level spacings.[21] These values are similar to those from μ-meson capture. A theoretical calculation by Brueckner, Lockett, and Rotenberg[22] gives an effective mass in Zr^{90} of 0.39, which also compares favorably with the values we get
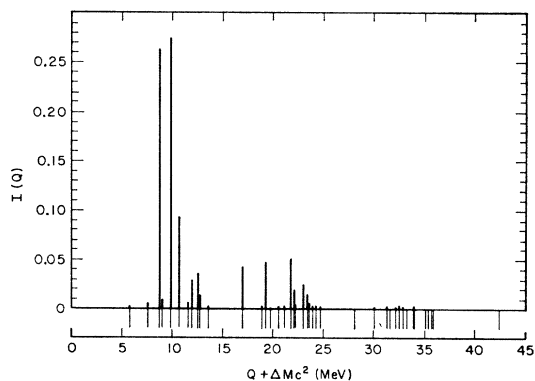

FIG. 10. Muon excitation of Ca^{40}. Shell-model calculation, harmonic-oscillator potential. $\langle n_{calc} \rangle = 0.744$; $\langle n_{expt} \rangle = 0.746 \pm 0.032$; $\chi^2 = 23$.

[21] E. Clementel and C. Villi, Nuovo Cimento 9, 950 (1958).
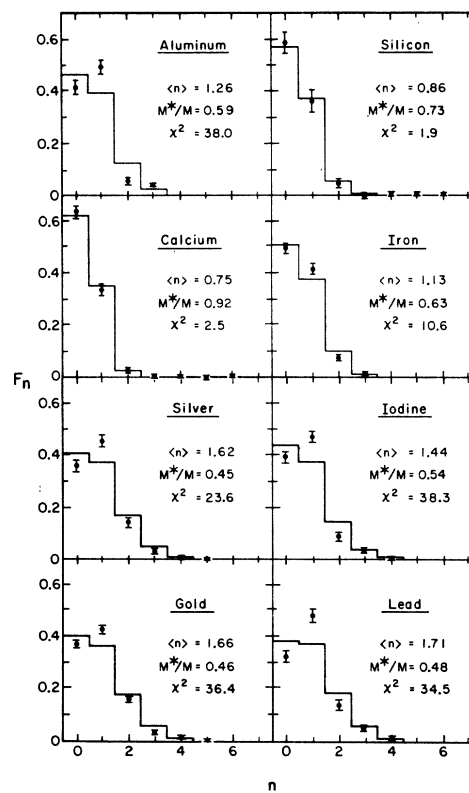[22] K. A. Brueckner, A. M. Lockett, and M. Rotenberg, Phys. Rev. 121, 255 (1961).

FIG. 11. Comparison of the observed neutron multiplicities with histograms calculated by using the Gaussian momentum distribution, $\alpha^2/2M = 20$ MeV.

for silver (which is our target closest in atomic weight to Zr^{90}).

The neutron multiplicity *distributions* predicted from our models are not in good agreement with the experimental values. The calculations, for example, uniformly predict fewer single-neutron emissions than observed (Fig. 11).

In the above discussion we have used a model that takes no account of direct emission of neutrons or of nuclear-surface effects.[5,6] Singer has shown that these effects may be important. He has estimated the fraction of directly emitted neutrons for the four heaviest elements used here, and a nucleon-clustering correction for silver. Direct emission increases the single-neutron yield at the expense of higher multiplicities. Singer's clustering calculation, which assumes some capture by nuclear-surface quasideuterons, provides a mechanism for enhancement of two-neutron emission. The above effects both tend to produce better agreement between calculation and experiment. (These arguments are of little consequence in the cases of Si and Ca because of the high binding energy of the second neutron and the resultant small likelihood of multiple-neutron emission.) Correcting for direct neutron emission (Table IX) decreases M^* by $\approx 12\%$ for the degenerate Fermi-gas model, by $\approx 25\%$ for the Fermi-gas model with

TABLE IX. Effective mass χ^2 and predicted multiplicity distributions corrected for Singer's direct emission and clustering.

Target	Direct-emission parameter	Clustering parameter	Effective mass M^*/M	χ^2	P_0	P_1	P_2	P_3	P_4	P_5
			Fermi gas, $\theta_f = 0$ MeV							
Ag	0.216	0	0.43	4.7	0.343	0.463	0.166	0.029		
I	0.199	0	0.45	20.2	0.378	0.474	0.136	0.012		
Au	0.157	0	0.34	27.9	0.333	0.458	0.179	0.030		
Pb	0.153	0	0.32	15.2	0.320	0.459	0.190	0.030		
Ag	0.216	0.144	0.45	9.5	0.333	0.472	0.175	0.019		
			Fermi gas, $\theta_f = 12$ MeV							
Ag	0.216	0	0.26	24.4	0.409	0.377	0.151	0.054	0.009	0.001
I	0.199	0	0.30	32.2	0.442	0.380	0.135	0.039	0.004	
Au	0.157	0	0.19	41.5	0.407	0.364	0.158	0.058	0.011	0.001
Pb	0.153	0	0.18	35.7	0.394	0.368	0.165	0.060	0.012	0.001
Ag	0.216	0.144	0.29	11.8	0.388	0.397	0.167	0.041	0.006	
			Gaussian, $\alpha^2/2M = 20$ MeV							
Ag	0.216	0	0.36	22.3	0.407	0.380	0.149	0.053	0.009	0.001
I	0.199	0	0.46	29.6	0.441	0.384	0.133	0.038	0.004	
Au	0.157	0	0.40	32.7	0.401	0.373	0.160	0.056	0.010	0.001
Pb	0.153	0	0.41	30.4	0.387	0.377	0.167	0.057	0.011	0.001
Ag	0.216	0.144	0.39	10.5	0.387	0.400	0.166	0.041	0.006	

$\theta_f = 12$ MeV, and by $\approx 15\%$ for the Gaussian, $\alpha^2/2M = 20$ MeV. This correction generally improves the fit with the multiplicity distribution for the 12-MeV Fermi-gas model and for the 20-MeV Gaussian model. For the degenerate Fermi-gas model it gives a substantial improvement in every case.

For silver the clustering correction increases M^* by 10% above the value based on the direct-emission correction (Table IX). The inclusion of both corrections gives significantly better agreement between experimental and calculated multiplicity values.

The nuclear radius ($r = r_0 A^{1/3}$) comes into our calculation through the proton and neutron Fermi momenta. Our calculated values of effective masses are insensitive to changes in r_0 ($\approx 5\%$ change in M^* for $r_0 = 1.2 \pm 0.1$ F). In common with Klein's calculation of μ^--capture rates in complex nuclei,[23] we find rather larger variations in M^*/M if the neutron and proton radii are assumed to be different. (A 0.1-F increase in r_0^n when $r_0^p = 1.2$ F gives an increase in M^*/M of ≈ 0.20.)

Any error introduced into our calculated results by ignoring proton emission (or direct neutron emission) has the effect of overestimating rather than underestimating effective masses.

The average nuclear excitation $\langle Q \rangle$ produced by muon capture appears to be a relatively insensitive function of the details of the excitation distribution and neutron-emission models. If we assume different values of $\langle n \rangle$ and calculate $\langle Q \rangle$ we find there is a linear relationship between $\langle n \rangle$ and $\langle Q \rangle$ very nearly independent of the model (Fermi gas or Gaussian) and the width of the momentum distribution. A typical example is given in Fig. 12. Only in the case of Ca is it not possible to fit

all of the points to a single straight line. For Ca the completely degenerate Fermi gas does not fit the line well, but neither does it fit the experimental multiplicity distributions nearly as well as either the Gaussian or the nondegenerate Fermi gas.

The average kinetic energy of the emitted neutron is reflected in our choice of nuclear temperature ($\langle KE \rangle = 2\theta_n$) and, as in Ref. 1, we have used a value of $\theta_n = 0.75$ throughout.

The value of θ_n has not been determined accurately for μ^- capture but is commonly deduced from low-energy fission and nuclear interactions. Turner[24] has measured
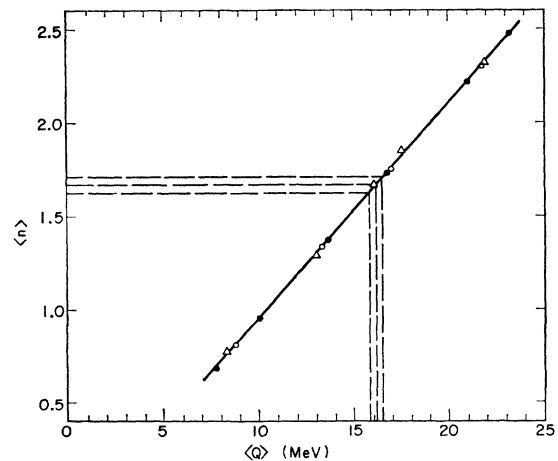

FIG. 12. Average neutron multiplicity $\langle n \rangle$ versus the average nuclear excitation $\langle Q \rangle$, (in gold) for both Gaussian and Fermi-gas momentum distributions at various temperatures and with various effective masses. The points can all be fitted with a single straight line.

[23] Robert H. Klein, Ph.D. thesis, Carnegie Institute of Technology, 1963 (unpublished).

[24] L. Turner, Ph.D. thesis, Carnegie Institute of Technology, 1964 (unpublished). These results were communicated to us by D. E. Hagge.

the μ^--capture neutron spectra for Ca and Pb in a hydrogen bubble chamber and shown that $\theta_n \lesssim 1$ MeV. From a comparison of the number of neutrons with $E \gtrsim 3$ MeV to the total neutron multiplicity for all of the targets used in this experiment, Hagge et al.[25] deduced $\theta_n \approx 0.5$ to 0.75 MeV. Around 0.75 MeV the variation $\Delta Q/\Delta\theta$ is approximately -2 for the most sensitive case, gold, so the assumed value of 0.75 MeV probably introduces an uncertainty in $\langle Q \rangle$ of no more than 0.5 MeV.

Values of $\langle Q \rangle$ determined from our experimental values of $\langle n \rangle$ are given in Table X. The statistical un-

TABLE X. Maximum excitation, average nuclear excitation, and average neutrino momentum.

Target	Maximum excitation, E_0 (MeV)	Average excitation, $\langle Q \rangle$ (MeV)	Average neutrino momentum $\langle p_\nu c \rangle$ (MeV)	$c(\langle p_\nu{}^4 \rangle)^{1/4}$ [a] (MeV)	$\langle p_\nu c \rangle/\mu'c^2$
Al	102.1	15.5	86.6	83.5	0.82
Si	100.0	13.3	86.7	84.5	0.82
Ca	102.8	11.7	91.1	89.5	0.87
Fe	99.7	14.5	85.2	82.5	0.82
Ag	99.8	17.5	82.3	78.1	0.82
I	98.7	15.6	83.0	79.8	0.83
Au	94.3	16.3	78.0	74.2	0.82
Pb	91.2	15.4	75.8	72.3	0.80

[a] The values given here are for the 20-MeV Gaussian. They are quite close to those for the 12-MeV Fermi gas and about 2 to 3 MeV less than the 0-MeV Fermi gas.

certainty in $\langle Q \rangle$ is less than ± 1 MeV (except for Si, ± 2 MeV). The uncertainty due to the model is probably not more than ± 1 MeV.

Also given in Table X are $\langle p_\nu \rangle$ and $(\langle p_\nu{}^4 \rangle)^{1/4}$. The latter values are more nearly those of interest in the calculation of muon-capture rates, but they are also more sensitive to the details of the excitation distribution and therefore not to be considered as experimentally determined but only presented for illustration.

If the average neutrino momentum is expressed as a fraction of the available energy, i.e., the μ mass reduced by its K-shell binding energy, we obtain the values in

the last column of Table X. With Ca as an exception this average neutrino momentum is quite uniform over a wide range of Z.

VI. CONCLUSIONS

With the models we have taken for neutron emission from μ-meson capture, reduced effective nuclear masses must be assumed in order to get agreement with our measured average neutron multiplicities.

The multiplicity distributions predicted by our model are not in quantitative agreement with the experimental results (except those for silicon and calcium). Inclusion of Singer's direct-emission correction for the four heaviest elements uniformly improved this agreement. For silver, his additional correction for nucleon clustering further improves the agreement except in the case of the degenerate Fermi gas. Our calculations for other elements, with reasonable values of the clustering parameter, did not lead to significant improvement.

The average nuclear excitation $\langle Q \rangle$ inferred from the average neutron multiplicity by means of evaporation theory is insensitive to the momentum distribution, effective mass, or other model parameters, the variation being no more than ± 1 MeV. When the average neutrino momentum, inferred from $\langle Q \rangle$, is expressed in units of a reduced μ mass (the rest-mass energy minus its K-shell binding energy), the result (with the exception of calcium) is constant—0.82 ± 0.01—over the wide range of atomic numbers covered. Of course, average values of higher moments of the neutrino momentum [such as $(\langle p_\nu{}^4 \rangle)^{1/4}$] become increasingly model sensitive and therefore less well determined by our measurements.

ACKNOWLEDGMENTS

[25] Donald E. Hagge, Jagdish S. Baijal, Justo A. Diaz, Selig N. Kaplan, and Robert V. Pyle, Bull. Am. Phys. Soc. 9, 725 (1964). Results expanded in paper 010, American Physical Society Winter Meeting, Berkeley, California, 1964 (unpublished).
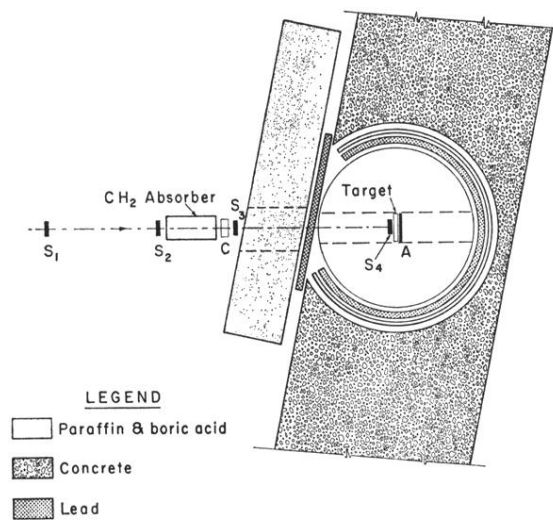
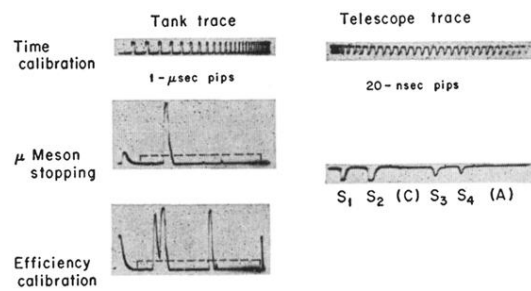FIG. 1. Experimental arrangement of the counter telescope and cadmium-loaded liquid-scintillator tank.

FIG. 3. Typical oscilloscope traces. For the tank trace, the dotted line represents the minimum height accepted and the time during which the neutron pulses were counted. On the telescope trace a muon stopping is signaled by the presence of pulses from counters S_2, S_3, and S_4, and the absence of Čerenkov and anticounter pulses (C and A).